A Finite Element Variational Multiscale Method for Steady-State Natural Convection Problem Based on Two Local Gauss Integrations

Yunzhang Zhang,[1,2] **Yanren Hou,**[3] **Haibiao Zheng**[3]

[1] *Department of Mathematics, Nanjing University, Nanjing 210093, People's Republic of China*

[2] *School of Mathematics and Statistics, Henan University of Science and Technology, Luoyang 471023, People's Republic of China*

[3] *School of Mathematics and Statistics and Center for Computational Geosciences, Xi'an Jiaotong University, Xi'an 710049, People's Republic of China*

Received 22 February 2012; accepted 20 June 2013
Published online 10 August 2013 in Wiley Online Library (wileyonlinelibrary.com).
DOI 10.1002/num.21811

In this article, supposing that the velocity, pressure, and temperature are approximated by the elements $P_2 - P_1 - P_2$, and applying the orthogonal projection technique, we introduce two Gauss integrations as a stabilizing term in the common variational multiscale (VMS) method and derive a new VMS (Two Gauss VMS) method for steady-state natural convection problem. Comparing with the common VMS method, the Two Gauss VMS method does not need to introduce any extra variable and reduces the degrees of freedom of the discrete system a lot, but gets the same stabilized result. The effectiveness and stability of the Two Gauss VMS method are further demonstrated through two numerical examples. Numer Methods Partial Differential Eq 30: 361–375, 2014

Keywords: natural convection problem; finite element method; variational multiscale method; two local gauss integrations

I. INTRODUCTION

Natural convection [1] is presented in many real situations, such as room ventilation, double glass window design, and so forth. Typically, fluid flow and heat transfer are governed by the partial

Correspondence to: Yunzhang Zhang, Department of Mathematics, Nanjing University, Nanjing 210093, P.R. China (e-mail: yzzmath@gmail.com)
Contract grant sponsor: NSFC; contract grant numbers: 11171269 and 11201369
Contract grant sponsor: Ph.D. Programs Foundation of Ministry of Education of China; contract grant number: 20110201110027
Contract grant sponsor: China Postdoctoral Science Foundation; contract grant number: 2013M531311
Contract grant sponsor: Henan Scientific and Technological Research Project; contract grant number: 132102310309
Contract grant sponsor: Doctor Fund of Henan University of Science and Technology; contract grant number: 09001625
Contract grant sponsor: Youth Scientific Foundation of Henan University of Science and Technology; contract grant number: 2012QN029

differential equation system of mass, momentum, and energy conservation, but in the case of natural convection, the so-called Boussinesq approximation is generally us. In this article, we present a new variational multiscale (VMS) method for buoyancy driven flows, namely, natural convection problem.

Let $\Omega \subset \mathbb{R}^2$ be a regular bounded open domain, the steady-state natural convection problem including solid media in dimensionless form is given by (see e.g., [2–4]):

$$\begin{cases} -Pr\Delta u + (u \cdot \nabla)u + \nabla p = Pr\ Ra\ \beta T, \quad \text{in } \Omega_f, \\ \text{div } u = 0 \quad \text{in } \Omega_f, \\ u = 0 \text{ on } \partial\Omega_f, u \equiv 0 \quad \text{in } \Omega - \Omega_f = \Omega_s, \\ -\nabla \cdot (k\nabla T) + (u \cdot \nabla)T = \gamma \quad \text{in } \Omega, \\ T = 0 \text{ on } \Gamma_T, \quad \dfrac{\partial T}{\partial n} = 0 \quad \text{on } \Gamma_B. \end{cases} \tag{1}$$

Here Ω_s and Ω_f are disjoint polyhedral domains, $\Gamma_T = \partial\Omega \setminus \Gamma_B$ which Γ_B is a regular open subset of $\partial\Omega$, and u, p, T denote the velocity, pressure, and temperature, respectively. β, γ, and n are the gravitational acceleration vector, forcing function, and the outward unit normal to Ω, respectively. The parameters Pr, Ra, $k > 0$ denote Prandtl number, Rayleigh number, and thermal conductivity parameter, respectively. Moreover, $k = k_f$ in Ω_f and $k = k_s$ in Ω_s, where k_f and k_s are two positive constants.

We denote by $(\cdot,\cdot)_\Omega$, $\|\cdot\|_{0,\Omega}$ the inner product and norm on $L^2(\Omega)$, $L^2(\Omega)^2$ or $L^2(\Omega)^{2\times 2}$. The standard Sobolev [5] space $H^\mu(\Omega)(\mu < \infty)$ is equipped with the norm $\|\cdot\|_{\mu,\Omega}$. Generally, Ω is omitted, that is, $(\cdot,\cdot) = (\cdot,\cdot)_\Omega$ and $\|\cdot\|_\mu = \|\cdot\|_{\mu,\Omega}$. The function spaces for u, p and T are defined, respectively, by

$$\begin{aligned} X &:= H_0^1(\Omega_f)^2 = \{v \in H^1(\Omega_f)^2 : v = 0 \text{ on } \partial\Omega_f\}, \\ Q &:= L_0^2(\Omega) = \{p \in L^2(\Omega), (p,1)_\Omega = 0\}, \\ W &:= \{S \in H^1(\Omega) : S = 0 \text{on} \Gamma_B\}. \end{aligned}$$

The corresponding variational formulation of problem (1) is followed: find $(u,p,T) \in X \times Q \times W$, for all $(v,q,S) \in X \times Q \times W$ such that

$$\begin{aligned} &Pr\ a(u,v) + c(u,u,v) + b(v,p) = Pr\ Ra\ d(T,v), \\ &b(u,q) = 0, \\ &\bar{a}(T,S) + \bar{c}(u,T,S) = (\gamma,S). \end{aligned} \tag{2}$$

Here, we used notations

$$a(u,v) = \int_{\Omega_f} \nabla u : \nabla v dxdy,$$

$$\bar{a}(T,S) = \int_{\Omega} k\nabla T \cdot \nabla S dxdy,$$

$$b(v,q) = -\int_{\Omega_f} q \text{div} v dxdy,$$

$$c(u,v,w)=\frac{1}{2}\int_{\Omega_f}((u\cdot\nabla)v\cdot w-(u\cdot\nabla)w\cdot v)dxdy,$$

$$\bar{c}(u,T,S)=\frac{1}{2}\int_{\Omega}((u\cdot\nabla)TS-(u\cdot\nabla)ST)dxdy,$$

$$d(T,v)=\int_{\Omega_f}T\beta\cdot vdxdy.$$

It is well-known that the solution of problem (2) is unique under some restrictions on the Rayleigh and Prandtl numbers [6]. If problem (2) is solved by standard Galerkin method, it may exhibit global spurious oscillations [7, 8] and may yield inaccurate approximation. One of the reasons is the dominance of convection terms. There are various stabilized methods for such problem. Among these methods, we only list some of them, such as, classical large eddy simulation approach in (see e.g., [9]); two-level stabilization scheme in (see e.g., [10]); VMS method (see e.g., [11–19]); and so forth. Recently, the projection-based stabilized method has been advanced for the natural convection problem [4, 20] and the Darcy–Brinkman equations in double-diffusive convection [21]. The philosophy of the projection-based stabilized method is to use projections into appropriate function spaces to decompose solution scales.

The two Gauss integrations technique was first used as a stabilizing term for the Stokes problem in (see e.g., [22–25]), where the authors applied them to overcome the inf-sup condition restriction between the velocity and pressure, and proved that the equal-order elements P_1-P_1 were compatible. While in [26, 27], we have developed a new VMS method by using two Gauss-integrations technique for incompressible flow. In this article, assuming that the velocity, the pressure, and the temperature are approximated by the elements $P_2-P_1-P_2$, and applying the orthogonal projection technique, we introduce two Gauss integrations as a stabilizing term in the common VMS method, and prove these two VMS methods are equivalent in mathematics. Namely, we formulate the Two Gauss VMS method for steady-state natural convection problem. The proposed method does not need to introduce any degrees of freedom, and can save computational cost a lot.

The article is organized as follows. In Section 2, we introduce some notations, and establish the Two Gauss VMS method for steady-state natural convection problem. Section 3 includes two numerical experiments to test and verify the stability and accuracy properties of the Two Gauss VMS method. Finally, conclusions are given in Section 4. The implementation of the stabilizing terms is given in Appendix section.

II. THE TWO GAUSS VMS METHOD

Let Ω^h be the uniformly regular family of triangulation of the domain $\overline{\Omega}$ where $\overline{\Omega}$ is the closure of Ω, and define the mesh parameter $h=\max_{K\in\Omega^h}\{h_K,h_K=\mathrm{diam}(K)\}$. For the velocity u, pressure p, and temperature T, we introduce the following finite element spaces to approximate them:

$$X_h=\{v_h\in X\cap C(\Omega)^2,v_h|_K\in P_2(K)^2,\forall K\in\Omega^h\},$$

$$Q_h=\{q_h\in Q\cap C(\Omega),q_h|_K\in P_1(K),\forall K\in\Omega^h\},$$

$$W_h=\{S_h\in W\cap C(\Omega),S_h|_K\in P_2(K),\forall K\in\Omega^h\},$$

where $P_r(K), r = 1, 2$ is the space of r^{th} order polynomial on K. Obviously, (X_h, Q_h) satisfies the discrete inf-sup condition [28]. To introduce the modified VMS method, we need to define some spaces:

$$R_0 = \{v_h \in L^2(\Omega), v_h|_K \in P_0(K), \forall K \in \Omega^h\},$$

where $P_0(K)$ is the space of all constant polynomial on K. Let $L = L^2(\Omega)$(or $L^2(\Omega)^{2\times 2}$), the finite element space $L_h = R_0(\Omega)^{2\times 2}$ and $M_h = R_0(\Omega)^2$.

With above notations, the projection-based stabilized method [4] of (2) reads: find $(u_h, p_h, T_h) \in X_h \times Q_h \times W_h$, and $(g_h, t_h) \in L_h \times M_h$ such that

$$\begin{aligned}
&Pr\ a(u_h, v_h) + \alpha_1((\nabla u_h - g_h), \nabla v_h) + c(u_h, u_h, v_h) + b(v_h, p_h) = Pr\ Ra\ d(T_h, v_h), \forall v_h \in X_h,\\
&b(u_h, q_h) = 0, \forall q_h \in Q_h, (g_h - \nabla u_h, l_h) = 0, \forall l_h \in L_h,\\
&\bar{a}(T_h, S_h) + \alpha_2((\nabla T_h - t_h), \nabla S_h) + \bar{c}(u_h, T_h, S_h) = (\gamma, S_h), \forall S_h \in W_h,\\
&(t_h - \nabla T_h, m_h) = 0, \forall m_h \in M_h,
\end{aligned} \tag{3}$$

where the stabilized parameters $\alpha_1 = \alpha_1(h)$ and $\alpha_2 = \alpha_2(h)$ are non-negative constant functions. The parameters α_1 and α_2 act only on the small scales. The scheme (3) is to add additional diffusion acting on all discrete velocity and temperature scales, and then to anti-diffuse on the resolvable scales. This is exactly the main idea of VMS method of Hughes et al. (see e.g., [12–14]), and we call the scheme (3) as the common VMS method. However, comparing with the continuous problem (2), the auxiliary spaces $L_h \times M_h$ and variables (g_h, t_h) are introduced in (3), it need to solve additional variables (g_h, t_h), which will increase the degrees of freedom of the discrete system a lot. This situation will be more serious for the three-dimensional (3D) problem.

Now, we introduce a new VMS method without adding any degrees of freedom. From (3), it is easy to see that the variable g_h is the L^2 projection of ∇u_h onto space L_h, and the variable t_h is the L^2 projection of ∇T_h onto space M_h, respectively. This technique was also used as a stabilizing factor for some convection-dominated problems (see e.g.,[15, 26, 29]). Thus, we can define an orthogonal projection operator $\Pi : L \to L_h$(orM_h) with the following properties (see e.g.,[17, 26, 28]):

$$\begin{aligned}
&((I - \Pi)l, \varrho_h) = 0, \forall l \in L, \quad \varrho_h \in L_h \quad (\text{or} \quad M_h),\\
&\|\Pi l\|_0 \le C\|l\|_0, \forall l \in L,\\
&\|(I - \Pi)l\|_0 \le Ch\|l\|_1, \forall l \in L \cap H^1(\Omega),
\end{aligned} \tag{4}$$

where the symbol I denotes identical operator. Using the properties of orthogonal projection operator Π, we can rewrite the scheme (3) as: find $(u_h, p_h, T_h) \in X_h \times Q_h \times W_h$, for all $(v_h, q_h, S_h) \in X_h \times Q_h \times W_h$ such that

$$\begin{aligned}
&Pr\ a(u_h, v_h) + \alpha_1((I - \Pi)\nabla u_h, (I - \Pi)\nabla v_h) + c(u_h, u_h, v_h) + b(v_h, p_h) = Pr\ Ra\ d(T_h, v_h),\\
&b(u_h, q_h) = 0,\\
&\bar{a}(T_h, S_h) + \alpha_2((I - \Pi)\nabla T_h, (I - \Pi)\nabla S_h) + \bar{c}(u_h, T_h, S_h) = (\gamma, S_h).
\end{aligned} \tag{5}$$

For the stabilized terms $\alpha_1((I - \Pi)\nabla u_h, (I - \Pi)\nabla v_h)$ and $\alpha_2((I - \Pi)\nabla T_h, (I - \Pi)\nabla S_h)$ in (5), to make them easy to implement, we supply the local stabilization form of the difference between a

TABLE I. Information on the grids and the numbers of degrees of freedom for the common VMS method.

$\sqrt{2}/h$	Cells	X_h	Q_h	W_h	L_h	M_h	Total
4	32	162	25	81	128	64	460
8	128	578	81	289	512	256	1716
16	512	2178	289	1089	2048	1024	6628
32	2048	8450	1089	4225	8192	4096	26,052

consistent and an under-integrated mass matrices on the local Gauss integrations at element level as follows (see e.g., [22–24]):

$$G(\sigma_h, \tau_h) = \alpha(a_r(\sigma_h, \tau_h) - a_1(\sigma_h, \tau_h)), \forall \sigma_h, \tau_h \in X_h \quad (\text{or} \quad W_h). \tag{6}$$

Here, $\alpha = \alpha_1(h)$ (or $\alpha_2(h)$) is a parameter and

$$\begin{aligned}
&a_r(\sigma_h, \tau_h) = \sigma_G^T M_r \tau_G, \quad a_1(\sigma_h, \tau_h) = \sigma_G^T M_1 \tau_G,\\
&\sigma_G^T = [\sigma_1, \sigma_2, \ldots, \sigma_N]^T, \quad \tau_G = [\tau_1, \tau_2, \ldots, \tau_N],\\
&M_{ij} = (\nabla\phi_i, \nabla\phi_j), \quad \sigma_h = \sum_{i=1}^{N} \sigma_i \phi_i, \quad \sigma_i = \sigma_h(x_i), \ \ \forall \sigma_h \in X_h(\text{or } W_h),\\
&M_r = (M_{ij}^r)_{N\times N}, M_1 = (M_{ij}^1)_{N\times N}, \quad i, j = 1, 2, \ldots, N,
\end{aligned}$$

and ϕ_i is the basis function of the velocity (temperature) on the domain Ω such that its value is one at node x_i and zero at other nodes; N is the dimension of X_h (or W_h); the symmetric and positive matrices M_{ij}^r ($r \geq 2$) and M_{ij}^1 are the mass matrices computed by using $r-$order and $1-$order Gauss integrations at element level, respectively; σ_i and τ_i ($i = 1, 2, \ldots, N$) are the values of σ_h and τ_h at the node x_i; σ_G^T is the transpose of the matrix σ_G. In details, for $\forall \sigma_h, \tau_h \in X_h(\text{or } W_h)$, the stabilized term can be rewritten as

$$G(\sigma_h, \tau_h) = \alpha \sum_K \left\{ \int_{K,r} \nabla\sigma_h \nabla\tau_h dxdy - \int_{K,1} \nabla\sigma_h \nabla\tau_h dxdy \right\}, \tag{7}$$

where $\int_{K,i} \varsigma(x, y)dxdy$ denotes an appropriate Gauss integral over K which is exact for polynomials of degree i ($i = 1, r$). In particular, for all test functions $\tau_h \in X_h$ (or W_h), $\nabla\sigma_h$ must be piecewise constant when $i = 1$.

Therefore, we derive a new stabilized VMS method (Two Gauss VMS method) as follows: find $(u_h, p_h, T_h) \in X_h \times Q_h \times W_h$ such that

$$\begin{aligned}
&Pr\ a(u_h, v_h) + c(u_h, u_h, v_h) + b(v_h, p_h) + G(u_h, v_h) = Pr\ Ra\ d(T_h, v_h),\\
&b(u_h, q_h) = 0,\\
&\bar{a}(T_h, S_h) + \bar{c}(u_h, T_h, S_h) + G(T_h, S_h) = (\gamma, S_h),
\end{aligned} \tag{8}$$

for all $(v_h, q_h, S_h) \in X_h \times Q_h \times W_h$.

We present the information on the grids and the numbers of the degrees of freedom for the common VMS method (3) in Table I and the Two Gauss VMS method (8) in Table II, respectively. It is easy to see that the common VMS method (3) will add more extra degrees of freedom in

TABLE II. Information on the grids and the numbers of degrees of freedom for the Two Gauss VMS method.

$\sqrt{2}/h$	Cells	X_h	Q_h	W_h	Total
4	32	162	25	81	268
8	128	578	81	289	948
16	512	2178	289	1089	3556
32	2048	8450	1089	4225	13,764

spaces $L_h \times M_h$ than the standard Galerkin method whereas h decreases, whereas the Two Gauss VMS method (8) does not add any extra degrees of freedom.

Remark 2.1. As afore mentioned, the Two Gauss VMS method (8) is only suitable for the elements $P_2 - P_1 - P_2$, our analysis and numerical tests are all carried out for this case. Now we establish the equivalence between the Two Gauss VMS method (8) and the common VMS method (3) for completeness. The reader can also see the proof in Ref. [26, 29]. To derive the equivalence, we only need to show the stabilized term $G(\sigma_h, \tau_h) = \alpha((I - \Pi)\nabla\sigma_h, (I - \Pi)\nabla\tau_h)$, $\forall\sigma_h, \tau_h \in X_h$ (or $\in W_h$). Using the properties (4) of Π, it suffices to prove that, at each element K

$$\int_{K,1} \nabla\sigma_h \nabla\tau_h dxdy = (\Pi\nabla\sigma_h, \Pi\nabla\tau_h)_K.$$

Let $q_i, i = 1, 2, 3$ denote the three vertices of K. For $\forall\sigma_h, \tau_h \in X_h$ (or W_h), we have $\nabla\sigma_h, \nabla\tau_h \in P_1(\Omega)^{2\times 2}$ (or $\in P_1(\Omega)^2$). Then, we obtain

$$\begin{aligned}\int_{K,1} \nabla\sigma_h \nabla\tau_h dxdy &= \int_{K,r} \nabla\sigma_h \left(\frac{q_1 + q_2 + q_3}{3}\right) \nabla\tau_h \left(\frac{q_1 + q_2 + q_3}{3}\right) dxdy \\ &= \int_{K,r} \frac{\nabla\sigma_h(q_1) + \nabla\sigma_h(q_2) + \nabla\sigma_h(q_3)}{3} \frac{\nabla\tau_h(q_1) + \nabla\tau_h(q_2) + \nabla\tau_h(q_3)}{3} dxdy \\ &= \int_{K,r} \Pi\nabla\sigma_h \Pi\nabla\tau_h dxdy = (\Pi\nabla\sigma_h, \Pi\nabla\tau_h)_K. \end{aligned} \tag{9}$$

The equivalence is true.

Remark 2.2. Now, we discuss how to choose the stabilized parameter $\alpha = \alpha_1(h)$ (or $\alpha_2(h)$). From [4], we see that the optimal error estimates for the velocity, the pressure, and the temperature can be obtained if and only if the stabilized parameters α_1 and α_2 are equal to $O(h^2)$ for the elements $P_2 - P_1 - P_2$. As the equivalence between the two VMS methods in Eq. (9), we directly choose the stabilized parameters $\alpha_1 = O(h^2)$ and $\alpha_2 = O(h^2)$, and omit the proof.

Remark 2.3. While taking the numerical tests, the stabilized terms in our VMS method (8) will be treated explicitly, that is,

$$G(\sigma_h^{(j)}, \tau_h) = \alpha \sum_K \left\{ \int_{K,r} \nabla\sigma_h^{(j)} \nabla\tau_h dx - \int_{K,1} \nabla\sigma_h^{(j-1)} \nabla\tau_h dx \right\},$$

for all $\sigma_h^{(j)}, \tau_h \in X_h$ (or W_h), where (j) denotes the number of Newton iteration. Meanwhile, the stabilization terms in (3) will be treated similarly.

III. NUMERICAL EXPERIMENTS

In this section, we give two numerical tests to validate the effectiveness of our VMS method (8). The first example is a known particular analytical solution, and the second one is natural convection in a squared cavity. All these computations are based on the package FreeFem++ (http://www. freefem.org/ff++ [30]), with some our additional codes. All nonlinear systems are solved by Newton method with stopping criteria 10^{-6}. More specifically, given an initial guess $(u_h^{(0)}, T_h^{(0)})$, we generate the sequence of iterates $(u_h^{(j)}, p_h^{(j)}, T_h^{(j)}) \in X_h \times Q_h \times W_h$ for $j \geq 1$ by solving the sequence of linear systems

$$\begin{aligned}
&Pr\ a(u_h^{(j)}, v_h) + c(u_h^{(j)}, u_h^{(j-1)}, v_h) + c(u_h^{(j-1)}, u_h^{(j)}, v_h) + b(v_h, p_h^{(j)}) + G(u_h^{j}, v_h) \\
&\quad = Pr\ Ra\ d(T_h^{(j)}, v_h) + c(u_h^{(j-1)}, u_h^{(j-1)}, v_h), \\
&b(u_h^{(j)}, q_h) = 0, \\
&\bar{a}(T_h^{(j)}, S_h) + \bar{c}(u_h^{(j)}, T_h^{(j-1)}, S_h) + \bar{c}(u_h^{(j-1)}, T_h^{(j)}, S_h) + G(T_h^{(j)}, S_h) \\
&\quad = (\gamma, S_h) + \bar{c}(u_h^{(j-1)}, T_h^{(j-1)}, S_h).
\end{aligned} \tag{10}$$

for all $(v_h, q_h, S_h) \in X_h \times Q_h \times W_h$. The linear systems are solved by UMFPACK solver. The stopping criterion is defined by $\max\{\|u_h^{(j)} - u_h^{(j-1)}\|, \|T_h^{(j)} - T_h^{(j-1)}\|\} < 10^{-6}$ for the iterative solver. We also record the iteration times (Iter) which reach the stopping criteria 10^{-6} in two VMS methods. The stabilized parameters $\alpha_1 = \alpha_2 = 2.0h^2$. The implementation of the stabilizing terms $G(u_h, v_h)$ and $G(T_h, S_h)$ in freefem++[30] code is presented in Appendix section.

A. An Analytical Solution

We choose the domain $\Omega = [0, 1]^2$ and the parameters $k = 1.0$, $Pr = 1.0$, and $Ra = 10,000$. The forcing function γ and boundary values of (u, p, T) are given such that the prescribed solution of problem (1) is

$$\begin{aligned}
p(x, y) &= 10(2x - 1)(2y - 1), \\
u_1(x, y) &= 10x^2(x - 1)^2y(y - 1)(2y - 1), \\
u_2(x, y) &= -10x(x - 1)(2x - 1)y^2(y - 1)^2, \\
T(x, y) &= u_1(x, y) + u_2(x, y), \quad u(x, y) = (u_1(x, y), u_2(x, y)).
\end{aligned}$$

The numerical results for this test are presented in Tables III–IV and Fig. 1. We see that the optimal convergence rates of (u, p, T) are obtained in terms of the elements $P_2 - P_1 - P_2$ for the two VMS methods. Besides, comparing Table III with Table IV, the numerical results are almost the same, which verify the two VMS methods are equivalent. However, Two Gauss VMS method needs less time, which implies that Two Gauss method (8) is more efficient than the common VMS method (3).

B. Natural Convection in a Squared Cavity

In this subsection, we consider a 2D problem of natural convection in an unit square cavity (see Fig. 2). The left and right walls are maintained at temperatures $T_H = 1$ and $T_C = 0$,

TABLE III. Numerical results of common VMS method for the numerical experiment A.

$\frac{\sqrt{2}}{h}$	$\|u-u^h\|_0$	$\|u-u^h\|_1$	$\|p-p^h\|_0$	$\|T-T^h\|_0$	$\|T-T^h\|_1$	Iter	CPU(s)
8	0.0111238	0.0854609	0.149398	1.69704e-4	0.00825468	9	6.911
12	0.00225232	0.0180354	0.033976	4.33071e-5	0.00358352	7	11.809
16	7.1826e-4	0.00635417	0.0136352	1.69488e-5	0.00199608	6	17.301
24	1.42687e-4	0.00181793	0.0048374	4.70282e-6	8.8048e-4	5	31.715
32	4.52658e-5	8.91453e-4	0.00258643	1.93292e-6	4.93912e-5	4	56.612

respectively, the horizontal walls are adiabatic (i.e. insulated, there is no heat transfer through these walls), no-slip boundary conditions are imposed for the fluid flow at all walls. Set the parameters $k = 1.0$, $Pr = 0.71$, $\gamma = 0$, and the Rayleigh numbers in the range $10^3 \leq Ra \leq 10^6$. For $Ra = 10^3, 10^4, 10^5$, and $Ra = 10^6$, we solve problems (3) and (8) on the uniform meshes of 11×11, 11×11, 21×21, and 32×32, respectively, where the mesh $m \times m$ denotes the domain $\Omega = [0, 1]^2$ by dividing into $m \times m$ squares and then drawing a diagonal in each square in the same direction.

Numerical results of this example are given in Tables V and VI, and Figs. 3–6. Tables V and VI present the maximum vertical velocity values at $y = 0.5$ and the maximum horizontal velocity values at $x = 0.5$ for different Rayleigh numbers, respectively, where the number "m" in parenthesis corresponds to the used mesh $m \times m$. It is easy to see that our results are concordant with the benchmark data [4, 31–34] even at coarser grid. We also present the vertical velocity distribution at $y = 0.5$ and the horizontal velocity distribution at $x = 0.5$ in Fig. 3, and give the variation of temperature at mid-height cavity $y = 0.5$ in Fig. 4, which are very popular graphical illustrations in the study of buoyancy-driven cavity type tests. We see that the differences in the profiles are getting bigger with the increase of Rayleigh numbers, which are concordant with the previous studies in [4, 34, 35].

The dimensionless parameter Nusselt number represents the rate of heat transfer along the vertical walls of the cavity. The local Nusselt number is calculated by $Nu_{\text{local}} = \pm\frac{\partial T}{\partial x}$, where the negative sign will be chosen at the hot wall and the positive sign will be chosen at the cold wall, respectively. The average Nusselt number at hot wall for different Rayleigh numbers are given in Table VII. The left and the right hand sides of Fig. 5 describe the variation of local Nusselt number at hot wall and cold wall for varying Rayleigh numbers, respectively. The results of Table VII and Fig. 5 are according with the benchmark solutions in [4, 31–33, 35].

The iso-u1 contours, iso-u2 contours, isotherms, isobars, and streamlines of the solutions (u, p, T) with Ra $= 10^3, 10^4, 10^5, 10^6$ are plotted in Fig. 6. It is easy to see that two horizontal eddies appear in the iso-u1 contours of Fig. 6 for lower Rayleigh numbers $Ra = 10^3, 10^4$, and these eddies are stretched to the upper-left and the lower-right corners for higher Rayleigh numbers

TABLE IV. Numerical results of Two Gauss VMS method for the numerical experiment A.

$\frac{\sqrt{2}}{h}$	$\|u-u^h\|_0$	$\|u-u^h\|_1$	$\|p-p^h\|_0$	$\|T-T^h\|_0$	$\|T-T^h\|_1$	Iter	CPU(s)
8	0.0111238	0.0854609	0.149398	1.69704e-4	0.00825468	9	3.651
12	0.00225232	0.0180354	0.033976	4.33071e-5	0.00358352	7	6.412
16	7.18259e-4	0.00635417	0.0136352	1.69488e-5	0.00199608	6	9.828
24	1.42687e-4	0.00181793	0.0048374	4.70282e-6	8.8048e-4	5	18.923
32	4.52658e-5	8.91453e-4	0.00258643	1.93292e-6	4.93912e-4	5	33.946

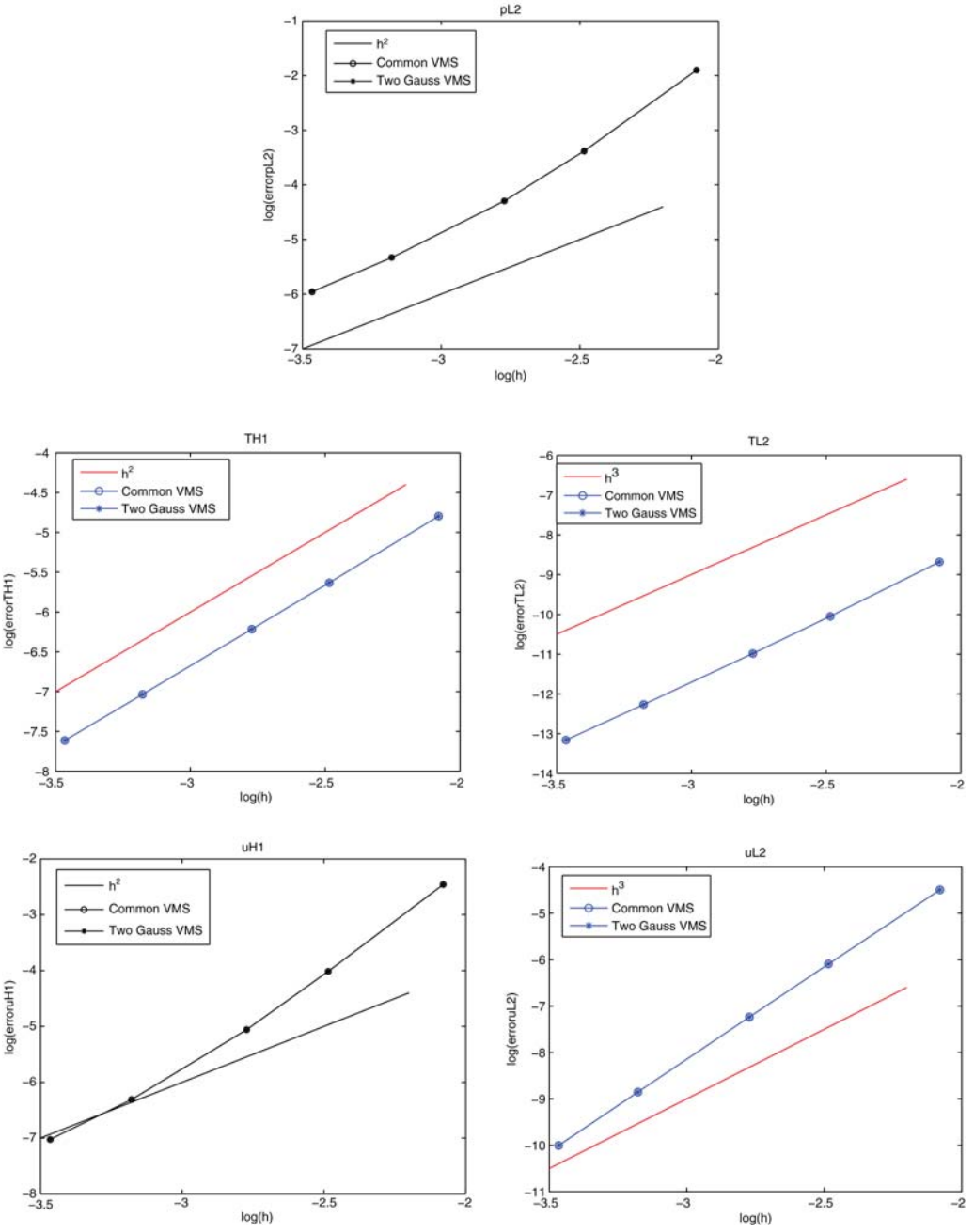

FIG. 1. Convergence analysis for the velocity, the pressure, and the temperature. From upper-left to lower-right, there are H^1 error for the velocity, L^2 error for the pressure, H^1 error for the temperature, L^2 error for the velocity, and L^2 error for the temperature, respectively. [Color figure can be viewed in the online issue, which is available at wileyonlinelibrary.com.]

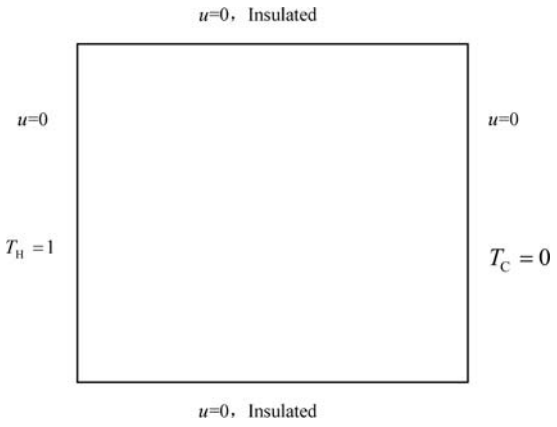

FIG. 2. Natural convection in cavity: schematic of the problem.

TABLE V. Comparison of maximum vertical velocity at $y = 0.5$ with mesh size used in computation for the numerical experiment B.

Ra	Two Gauss	Ref. [4]	Ref. [31]	Ref. [32]	Ref. [33]	Ref. [34]
10^4	19.46(11)	19.91(11)	19.51(41)	19.63(71)	19.90(71)	19.79(101)
10^5	68.31(21)	70.60(21)	68.22(81)	68.85(71)	70(71)	70.63(101)
10^6	216.36(32)	228.12(32)	216.75(81)	221.6(71)	228(71)	227.11(101)

TABLE VI. Comparison of maximum horizontal velocity at $x = 0.5$ with mesh size used in computation for the numerical experiment B.

Ra	Two Gauss	Ref. [4]	Ref. [31]	Ref. [33]	Ref. [34]
10^4	16.21(11)	15.90(11)	16.18(41)	16.10(71)	16.10(101)
10^5	34.68(21)	33.51(21)	34.81(81)	34(71)	34(101)
10^6	64.65(32)	65.52(32)	65.33(81)	65.40(71)	65.40(101)

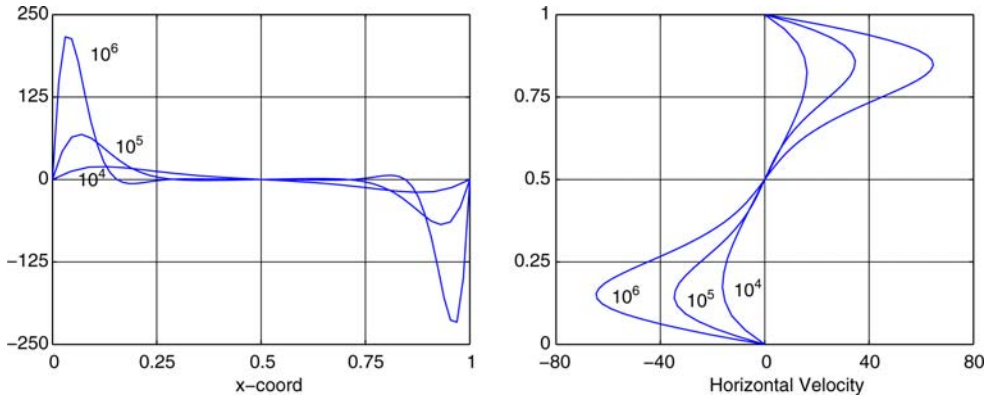

FIG. 3. Natural convection cavity: comparison of vertical velocity at the mid-height (left) and horizontal velocity at mid-width (right) for varying Rayleigh numbers, obtained by using Two Gauss VMS method. [Color figure can be viewed in the online issue, which is available at wileyonlinelibrary.com.]

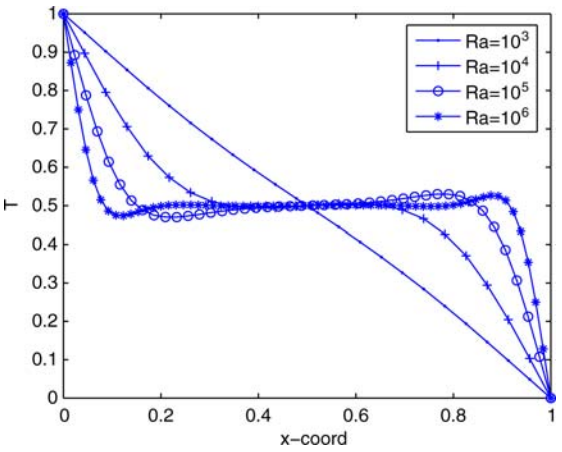

FIG. 4. Natural convection cavity: comparison of temperature at mid-height cavity $y = 0.5$ for varying Rayleigh numbers, obtained by using Two Gauss VMS method. [Color figure can be viewed in the online issue, which is available at wileyonlinelibrary.com.]

$Ra = 10^5, 10^6$. For lower Rayleigh numbers $Ra = 10^3, 10^4$, there are two vertical eddies appear in the iso-u2 contours of Fig. 6. With the increase of Rayleigh numbers, these vertical eddies become closer to the hot and cold walls. The isotherm of Fig. 6 is nearly linear with the vertical contours for $Ra = 10^3$, which indicates that the heat transfer is almost entirely in the form of conduction. While for higher Rayleigh numbers $Ra = 10^5, 10^6$, the growth of the boundary layer along the wall dominates, which shows that the hot fluid has been carried to the cold wall. From the isobar patterns of Fig. 6, we see that the pressure differences increase gradually with Rayleigh number increasing. From the streamline patterns of Fig. 6, it is clear that circular vortex at the cavity center begin to deform into an ellipse and then break up into two vortices tending to approach to the corners differentially heated sides of the cavity as Rayleigh number increases. We remark that these results of Fig. 6 are according with the results of [1, 31–35].

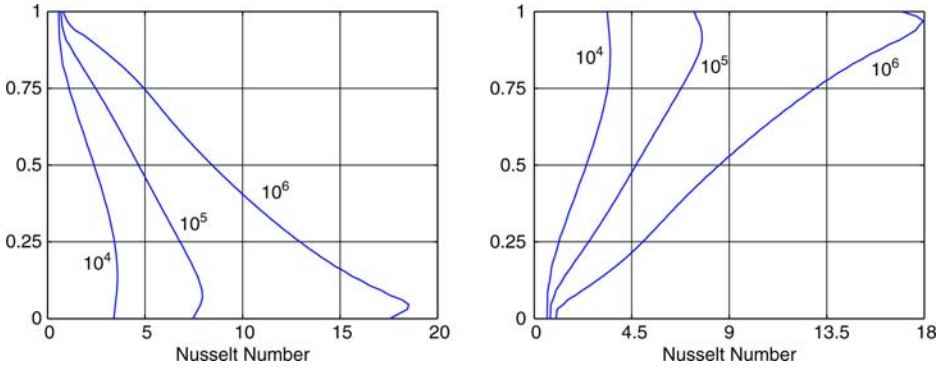

FIG. 5. Natural convection cavity: Nusselt number along the hot wall (left) and the cold wall (right) for varying Rayleigh numbers, obtained by using Two Gauss VMS method. [Color figure can be viewed in the online issue, which is available at wileyonlinelibrary.com.]

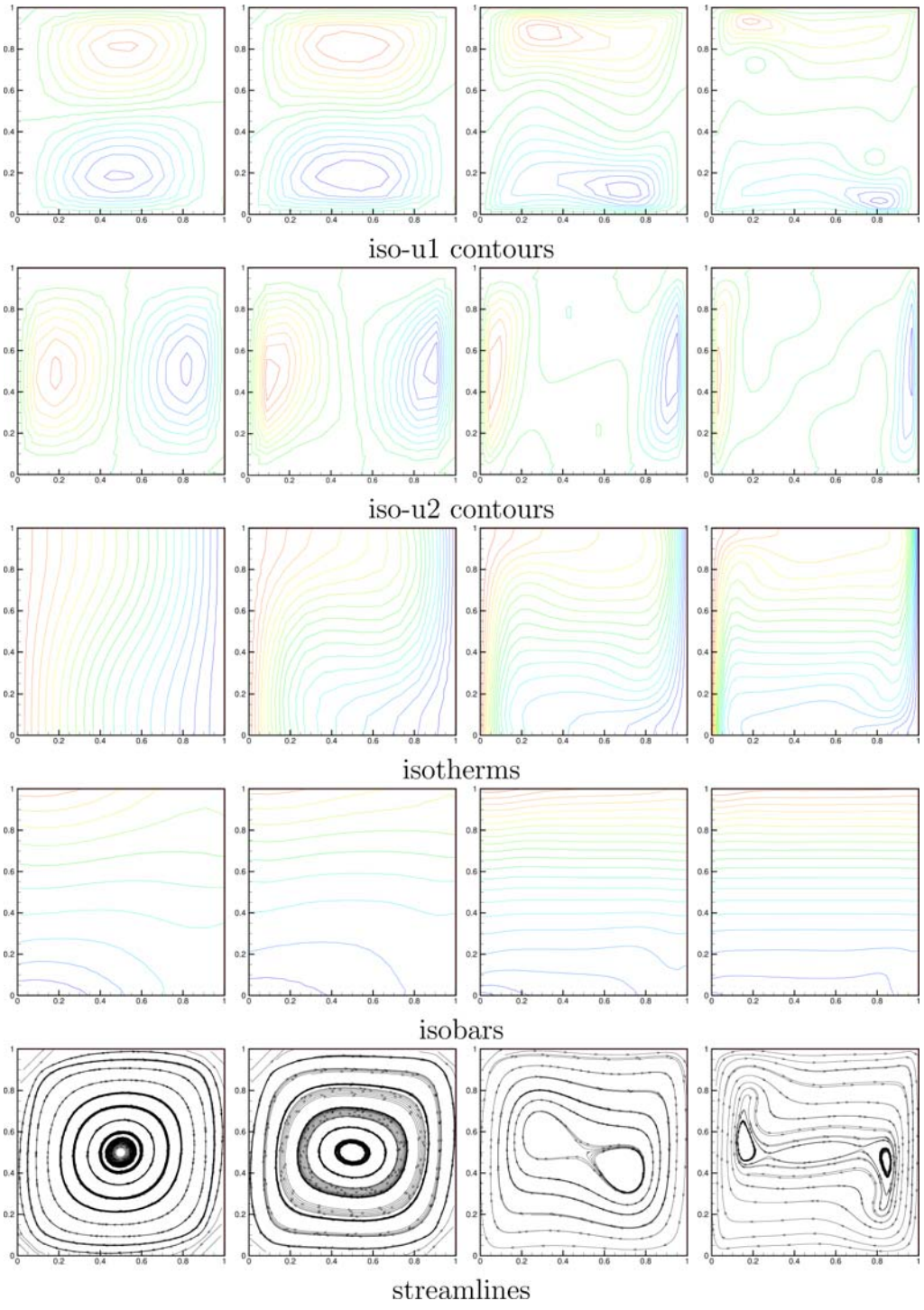

FIG. 6. Iso-u1 contours, iso-u2 contours, isotherms, isobars, streamlines from top to bottom, and with $\mathrm{Ra} = 10^3, 10^4, 10^5, 10^6$ from left to right for Natural convection problem, respectively. [Color figure can be viewed in the online issue, which is available at wileyonlinelibrary.com.]

TABLE VII. Comparison of average Nusselt number on the vertical boundary of the cavity at $x = 0$ with mesh size used in computation for the numerical experiment B.

Ra	Two Gauss	Ref. [4]	Ref. [31]	Ref. [32]	Ref. [33]	Ref. [34]
10^4	2.23(11)	2.15(11)	2.24(41)	2.24(71)	2.08(71)	2.25(101)
10^5	4.55(21)	4.35(21)	4.52(81)	4.52(71)	4.30(71)	4.59(101)
10^6	9.01(32)	8.83(32)	8.92(81)	8.82(71)	8.74(71)	8.97(101)

IV. CONCLUSIONS

In this article, we have proposed Two Gauss VMS method for steady-state natural convection problem, which is proved to be equivalent to the common VMS in mathematics, but it does not introduce any additional degrees of freedom in the discrete system. Thus, Two Gauss VMS method is efficient when implementing and can save computational cost a lot. The numerical experiments verified the theoretical predictions.

There are many open questions including the possible extension of the method to time-dependent problems and more extensive testing, and so forth.

APPENDIX

The Appendix presents the implementation of the stabilizing term $G(\sigma_h, \tau_h)$ in freefem++ code, for details, please see [30].

```
mesh Th=square(z,z,[0+(1.0-0)*x,0+(1.0-0)*y]);
\\ defining the mesh on [0, 1]^2
fespace Xh(Th, P2);
\\ definition of the velocity component finite element space
Xh u1,u2,v1,v2; \\ unknown and test functions
Xh u01,u02;
\\ here u01, u02 denote the above step iterative value of u1,u2, respectively.
fespace Qh(Th,P1); \\ definition of the pressure finite element space
Qh p,q; \\unknown and test function
fespace Wh(Th,P2);\\definition of the temperature finite element space.
Wh T,S;\\ unknown and test function
Wh T0;\\here T0 denotes the above step iterative value of T
...
problem TwoGaussVMS([u1,u2,p,T],[v1,v2,q,S],solver=UMFPACK)
\\definition of the problem
=int2d(Th)(Pr*(dx(u1)*dx(v1)+dy(u1)*dy(v1)+dx(u2)*dx(v2)+dy(u2)*dy(v2))
\\bilinear term: Pr a(u,v) = Pr ∫_{Ω_f} ( ∂u1/∂x ∂v1/∂x + ∂u1/∂y ∂v1/∂y + ∂u2/∂x ∂v2/∂x + ∂u2/∂y ∂v2/∂y ) dxdy
+int2d(Th)(k*(dx(T)*dx(S)+dy(T)*dy(S)))
\\bilinear term: ā(T,S) = ∫_Ω ( k * ( ∂T/∂x ∂S/∂x + ∂T/∂y ∂S/∂y ) )
+...
+int2d(Th,qft=qf2pT)(2.0*hTriangle*hTriangle*(dx(u1)*dx(v1)
+dy(u1)*dy(v1) +dx(u2)*dx(v2)+dy(u2)*dy(v2)))
\\ hTriangle denotes the size of the current triangle K(diam(K))
-int2d(Th,qft=qf1pT)(2.0*hTriangle*hTriangle*(dx(u01)*dx(v1)
```

+dy(u01)*dy(v1) +dx(u02)*dx(v2)+dy(u02)*dy(v2)))
\\stabilizing term: $G(u_h, v_h)$, here the parameter $\alpha_1(h) = 2.0 * (hTriangle)^2$
+int2d(Th,qft=qf2pT)(2.0*hTriangle*hTriangle*(dx(T)*dx(S)+dy(T)*dy(S)))
-int2d(Th,qft=qf1pT)(2.0*hTriangle*hTriangle*(dx(T0)*dx(S)+dy(T0)*dy(S)))
\\stabilizing term: $G(T_h, S_h)$, here the parameter $\alpha_2(h) = 2.0 * (hTriangle)^2$
+...

The authors would like to thank the editor and the anonymous referees for their valuable comments, which led to great improvements in content.

References

1. M. Benítez and A. Bermùdez, A second order characteristics finite element scheme for natural convection problems, J Comput Appl Math 235 (2011), 3270–3284.
2. J. Boland and W. Layton, An analysis of the finite element method for natural convection problems, Numer Methods Partial Differ Equ 2 (1990), 115–126.
3. J. Boland and W. Layton, Error analysis for finite element methods for steady natural convection problems, Numer Funct Anal Optim 11 (1990), 449–483.
4. A. Cibik and S. Kaya, A projection based stabilized finite element method for steady-state natural convection problem, J Math Anal Appl 381 (2011), 469–484.
5. R. A. Adams, Sobolev space pure and applied mathematics, Vol. 65, Academic press, New York, 1975.
6. P. H. Rabinowitz, Existence and nonuniqueness of rectangular solutions of the Benard problem, Arch Ration Mech Anal 29 (1968), 32–57.
7. P. M. Gresho, M. Lee, S. T. Chan, and R. L. Sani, Solution of time dependent, incompressible Navier-Stokes and Boussinesq equations using the Galerkin finite element method, Lecture Notes in Math., Vol. 771, Springer-Verlag, Berlin/Heidelberg/New York, 1980, pp. 203–222.
8. H. Melhem, Finite element approximation to heat transfer through combined solid and fluid media, PhD thesis, University of Pittsburgh, 1987.
9. V. John, Large eddy simulation of turbulent incompressible flows, analytical and numerical results for a class of LES models, Lecture notes in computational science and engineering, Vol. 34, Springer, Berlin, Heidelberg, New York, 2004.
10. R. Becker and M. Braack, A two-level stabilization scheme for the Navier-Stokes equations, M. Feistaue, editor, Numerical Mathematics and Advanced Applications, ENUMATH 2003, Springer-Verlag, Berlin, 2004, pp. 123–130.
11. J.-L. Guermond, Stabilization of Galerkin approximations of transport equations by subgrid modeling, M2AN Math Model Numer Anal 33 (1999), 1293–1316.
12. T. J. R. Hughes, L. Mazzei, and A. A. Oberai, The multiscale formulation of large eddy simulation: decay of homogeneous isotropic turbulence, Phys Fluids 13 (2001), 505–511.
13. T. J. R. Hughes, L. Mazzei, and K. E. Jensen, Large eddy simulation and the variational multiscale method, Comput Vis Sci 3 (2000), 47–59.
14. T. J. R. Hughes, Multiscale phenomena: Green's functions, the Dirichlet-to-Neumann formulation, subgrid-scale models bubbles and the origin of stabilized methods, Comput Methods Appl Mech Eng 127 (1995), 387–401.
15. W. J. Layton, A connection between subgrid scale eddy viscosity and mixed methods, Appl Math Comput 133 (2002), 147–157.
16. S. Kaya, W. layton, and B. Riviere, Subgrid stabilized defect correction methods for the Navier-Stokes equations, SIAM Numer Anal 44 (2006), 1639–1654.

17. V. John and S. Kaya, A finite element variational multiscale method for the Navier Stokes equations, SIAM J Sci Comput 26 (2005), 1485–1503.

18. S. Kaya and B. Riviere, A two-grid stabilization method for solving the steady-state Navier-Stokes equations, Numer Methods Partial Differ Equ 3 (2006), 728–743.

19. V. John and S. Kaya, Finite element error analysis of a variational multiscale method for the Navier-Stokes equations, Adv Comput Math 28 (2008), 43–61.

20. A. Cibik and S. Kaya, Finite element analysis of a projection-based stabilization method for the Darcy-Brinkman equations in double-diffusive convection, Appl Numer Math 64 (2013), 35–49.

21. J. Lowe and G. Lube, A projection-based variational multiscale method for Large-Eddy simulation with application to non-isothermal free-convection problems, Math Models Methods Appl Sci 22 (2012), 1150011 (31 pages).

22. J. Li and Y. He, A stabilized finite element method based on two local Gauss integrations for the Stokes equations, J Comp Appl Math 214 (2008), 58–65.

23. Y. He and J. Li, A stabilized finite element method based on two local polynomial pressure projection for the stationary Navier-Stokes equations, Appl Numer Math 58 (2008), 1503–1514.

24. J. Li and Z. Chen, A new local stabilized nonconforming finite element method for the Stokes equations, Computing 82 (2008), 157–170.

25. H. Zheng, L. Shan, and Y. Hou, A quadratic equal-order stabilized method for Stokes problem based on two local Gauss integrations, Numer Methods Partial Differ Equ 26 (2010), 1180–1190.

26. H. Zheng, Y. Hou, F. Shi, and Lina Song, A finite element variational multiscale method for incompressible flows based on two local Gauss integrations, J Comput Phys 228 (2009), 5961–5971.

27. Y. Hou, H. Zheng, and F. Shi, Adaptive variational multiscale methods for incompressible flow based on two local Gauss integrations, J Comput Phys 229 (2010), 7030–7041.

28. R. Temam, Navier-Stokes equation: theory and numerical analysis (Third edition), North-Holland, Amsterdam, New York, Oxford, 1984.

29. K. Wang, A new discrete EVSS method for the viscoelastic flows, Comput Math Appl 65 (2013), 609–615.

30. F. Hecht, O. Pironneau, A. LeHyaric, and K. Ohtsuka, FreeFem++ (2011). Available at: http://www.freefem.org/ff++.

31. D. de Vahl Davis, Natural convection of air in a square cavity: a benchmark solution, Int J Numer Methods Fluids 3 (1983), 249–264.

32. N. Massarotti, P. Nithiarasu, and O. C. Zienkiewicz, Characteristic-based-split (CBS) algorithm for incompressible flow problems with heat transfer, Int J Numer Methods Heat Fluid Flow 8 (1998), 969–990.

33. M. T. Manzari, An explicit finite element algorithm for convective heat transfer problems, Int J Numer Methods Heat Fluid Flow 9 (1999), 860–877.

34. D. C. Wan, B. S. V. Patnaik, and G. W. Wei, A new benchmark quality solution for the buoyancy-driven cavity by discrete singular convolution, Numer Heat Transfer Part B 40 (2001), 199–228.

35. M. El-Amrani and M. Seaïd, Numerical simulation of natural and mixed convection flows by galerkin-characteristic method, Int J Numer Meth Fluids 53 (2007), 1819–1845.